Journal of Materials Chemistry A

Single Iron Atoms Stabilized by Microporous Defects of Biomass-Derived Carbon Aerogels as High-Performance Electrocatalysts for Aluminium-Air Battery

Journal:	*Journal of Materials Chemistry A*
Manuscript ID	TA-ART-06-2019-005981.R1
Article Type:	Paper
Date Submitted by the Author:	22-Jul-2019
Complete List of Authors:	He, Ting; Central South University, Chemistry and Chemical Engineering Zhang, Yaqian; University of Alberta, Chemical and Materials Engineering Chen, Yang; Central South University Zhang, Zhenzhu; Central South University Wang, Hai-Yan; Central South University, Chemistry and Chemical Engineering Hu, Yongfeng; University of Saskatchewan Liu, Min; Central South University, Department of Physics Pao, Chih-Wen; NSRRC, Chen, Jeng-Lung; National Synchrotron Radiation Research Center, Chang, Lo-Yueh; National Synchrotron Radiation Reseac Center Sun, Zhifang; Central South University, Xiang, Juan; Central South University, College of Chemistry and Chemical Engineering Zhang, Yi; Central South University, Chemistry and Chemical Engineering Chen, Shaowei; University of California Santa Cruz, Chemistry and Biochemistry

Journal of
Materials Chemistry A

ARTICLE

Single iron atoms stabilized by microporous defects of biomass-derived carbon aerogels as high-performance cathode electrocatalysts for aluminum-air batteries

Received 00th January 20xx,
Accepted 00th January 20xx

DOI: 10.1039/x0xx00000x

Ting He,[a,b] Yaqian Zhang,[c] Yang Chen,[a] Zhenzhu Zhang,[a] Haiyan Wang,[a] Yongfeng Hu,[d] Min Liu,[e] Chih-Wen Pao,[f] Jeng-Lung Chen,[f] Lo Yueh Chang,[g,h] Zhifang Sun,[a]* Juan Xiang, [a] Yi Zhang[a]* and Shaowei Chen[b]*

Atomically dispersed metal catalysts have demonstrated superb electrocatalytic activity because of optimal atom efficiency. However, a rational design of low-cost, high-performance single atom catalysts remains a great challenge due to the elusive chemical reactions of the formation of metal active sites. In this work, biomass hydrogel is prepared as a template for mass production of three-dimensional carbon aerogel-supported single metal atom catalysts. By tailoring the structure of the hydrogel templates, the obtained carbon aerogels exhibit an increase of microporous defects which capture and stabilize isolated metal atoms and minimize aggregation during pyrolysis. Extended X-ray absorption fine structure, Mössbauer spectroscopy, and nitrogen adsorption-desorption isotherm measurements indicate that single metal centers of FeN_4 are formed and embedded within the hierarchical porous carbon frameworks. The obtained composites exhibit an outstanding catalytic activity towards oxygen reduction in alkaline media, with a high onset potential of +1.05 V and half-wave potential of +0.88 V, as well as excellent durability. Remarkably, when used as the cathode in an aluminum-air battery, this battery achieves an ultrahigh open-circuit voltage of 1.81 V, large power density of 181.1 mW cm^{-2} and stable discharge voltage of 1.70 V at 20 mA cm^{-2}, markedly better that with commercial Pt/C as the cathode catalyst.

Introduction

Because of the rapid depletion of non-renewable fossil fuels and the detrimental impacts on the environment, development of sustainable clean energy technologies, such as fuel cells, and metal-air batteries, have been attracting extensive interest.[1-6] Nevertheless, the commercialization of fuel cells and metal-air batteries have been primarily hampered by the high costs and poor durability of platinum-based cathode materials.[7-9] Ternary metal–nitrogen–carbon (MNC) nanocomposites have been hailed as viable alternatives to Pt-based catalysts, owing to their competitive catalytic performance, strong poison resistance, and enhanced durability.[10-14] Recent studies of MNC catalysts for oxygen reduction reaction (ORR) are generally focused on two strategies. One is to design unique metal sites with optimized activity, such as single metal atoms, metal nanoclusters, bimetals and metal/metal oxide catalysts.[15-23] In these studies, single metal atom catalysts are of particular interest as the utilization of metal sites is maximized.[24-27] The other strategy focuses on the development of new carbon substrates that are electrically conductive for electron transport and possess hierarchical pores for mass transport. Indeed, a series of unique carbon substrates have been developed to improve these physicochemical properties, such as heteroatom-doped graphene/carbon nanotube, graphitic carbon nitride, hierarchical porous carbon, etc.[28-33] It is well recognized that 3D carbon aerogels with a hierarchical porous structure and high degree of graphitization possess a large surface area, rich mass transport channels and excellent electrical conductivity, and hence may serve as ideal carbon substrates.[34-37] However, to the best of our knowledge, reports of ORR catalysts based on single metal atoms embedded within 3D porous carbon aerogels have been scarce.[38] Herein, we integrate the two strategies described above and demonstrate that the strong electronic coupling of single metal atoms with 3D porous carbon aerogels can be exploited for the

[a] *Hunan Provincial Key Laboratory of Efficient and Clean Utilization of Manganese Resources, School of Chemistry and Chemical Engineering, Central South University, Changsha 410083 (China), allensune@gmail.com; yzhangcsu@csu.edu.cn*
[b] *Department of Chemistry and Biochemistry, University of California, 1156 High Street, Santa Cruz, California 95064 (United States), shaowei@ucsc.edu*
[c] *Department of Chemical and Materials Engineering, University of Alberta, Edmonton, Alberta T6G 1H9 (Canada)*
[d] *Canadian Light Source, Saskatoon, Saskatchewan (Canada)*
[e] *Institute of Super-Microstructure and Ultrafast Process in Advanced Materials, School of Physics and Electronics, Central South University, Changsha 410083 (China)*
[f] *X-ray Absorption Group, National Synchrotron Radiation Research Center, Hsinchu 30076 (Taiwan, Republic of China)*
[g] *Institute of Functional Nano & Soft Materials (FUNSOM), Soochow University, Suzhou, Jiangsu 215123 (China)*
[h] *Soochow University- Western University Centre for Synchrotron Radiation Research, Suzhou, Jiangsu 215123 (China)*
Electronic Supplementary Information (ESI) available: [details of any supplementary information available should be included here]. See DOI: 10.1039/x0xx00000x

development of high-performance ORR electrocatalysts, and large-scale production is possible by using abundant biomass.

Experimentally, hydrogels are first prepared that are composed of 3D cross-linked networks with water-rich interiors.[39, 40] Such well-organized chemical networks can not only be easily processed into 3D porous carbon aerogels, but also provide multitudinous sites to anchor transition metals into the carbon framework during pyrolysis. Among the wide variety of hydrogels, biomass hydrogels are most promising, because they are abundant in the biosphere, renewable, low-cost and environmentally friendly. In this study, we demonstrate that indeed biomass hydrogels can be used as starting precursors for the preparation of single metal atoms supported by 3D porous carbon aerogels, and the procedure is scalable. There are various immediate advantages in such a strategy. (a) The hierarchical porous carbon aerogels entail highly active single metal atom sites and rich electron/mass transfer channels. (b) Within the carbon aerogels, the single metal atoms are captured and stabilized by microporous defects that are *in situ* produced by tailoring hydrogel precursors.[41] (c) The renewability, low costs and flexibility of biomass hydrogels render it possible to achieve large-scale production of the electrocatalysts.

Experimental Section

Chemicals

Potassium hydroxide (KOH), iron(II) chloride tetrahydrate ($FeCl_2{\cdot}4H_2O$), sodium stanate (Na_2SnO_3), indium(III) hydroxide ($In(OH)_3$), zinc oxide (ZnO), and iron(II) phthalocyanine (FePc) were all purchased from Aladdin Reagents (Shanghai, China). Perchloric acid ($HClO_4$) and ammonium hydroxide were obtained from Chengdu Xiya Reagent Chemical Technology Co. Ltd. Nafion solution was purchased from Sigma-Aldrich, commercial Pt/C (20 wt. %) from Johnson Matthey, and polytetrafluroethylene (PTFE, 60 wt.%, D-210C) from DaJin Chemical Trade Co. All other reagents were of analytical grade, and ultrapure water (MillQ, 18.2 MΩ cm) was used throughout this study.

Sample preparation

Lotus root-derived hydrogels (LR-Si/Me-Fe) were first prepared by dispersing lotus root powders (250 mg), SiO_2 nanoparticles (100 mg) and $FeCl_2$ (0.2 M, 450 µL) in a melamine solution (4 mg mL^{-1}, 6 mL) under ultrasonication in a boiling water bath, and then subject to freeze drying to obtain a xerogel, followed by controlled pyrolysis in a high-purity Ar atmosphere at 850 °C for 3 h. The SiO_2 nanoparticle templates were then removed by HF etching, and the sample underwent a second pyrolytic treatment (950 °C, 1 h) to increase the electrical conductivity. The resulting Fe,N-codoped carbon aerogel composite was denoted as NCA_{LR}/Fe.

Two additional samples were prepared in the same fashion but by using sweep potato and potato as the starting biomass, and the final samples were referred to as NCA_{SP}/Fe and NCA_{PT}/Fe, respectively.

Three control samples were also prepared by following the same method, but by using lotus root-SiO_2 nanoparticles, lotus root-SiO_2 nanoparticles/melamine, lotus root-SiO_2 nanoparticles/$FeCl_2$ biomass hydrogels as the respective precursor. The resulting samples were carbon aerogel (CA_{LR}), N-doped carbon aerogel (NCA_{LR}), and carbon aerogel with atomically dispersed Fe (CA_{LR}/Fe), respectively.

Characterization

Scanning electron microscopy (SEM) studies were performed with a Hitachi S-4800 field-emission SEM instrument, and transmission electron microscopy (TEM) images were acquired with a T20 FEI TECNA1 G2 scope. Scanning transmission electron microscopy (STEM) with energy-dispersive X-ray spectroscopy (EDX) studies were performed using a JEOL JEM-ARM200CF with probe aberration-corrected STEM. X-ray powder diffraction (XRD) and X-ray photoelectron spectroscopy (XPS) measurements were carried out with a D/max 2550 X-ray Powder Diffractometer (Japan) and an ESCALAB 250Xi X-ray Photoelectron Spectrometer (Thermo Fisher-VG Scientific), respectively. Raman spectra were acquired with a Renishaw inVia Raman Microscope. Nitrogen adsorption–desorption isotherms were acquired at 77 K with a Micromeritics ASAP 2020 surface area and porosity analyzer. Inductively coupled plasma-optical emission spectrometry (ICP-OES) analysis was performed on SPECTRO BLUE SOP. Mössbauer spectra were obtained with a Wissel Mössbauer system. X-ray absorption spectroscopic (XAS) measurements were performed at the Quick-EXAFS beamline of the Taiwan Photon Source in transmission mode and the results were analyzed using Athena program. Voltammetric measurements were conducted with an RST 5200F electrochemical workstation. Rotating disk electrode (RDE, Pine Research Instrument) tests were carried out at the rotation rates of 400 to 1600 rpm.

Fabrication of home-made aluminium-air battery

To assemble an Al-air battery, a 6M KOH solution containing 0.01 M Na_2SnO_3, 0.0005 M $In(OH)_3$, and 0.0075 M ZnO (as corrosion inhibitor) was used as electrolyte. An aluminium plate was used as the anode, and the air cathode was composed of three layers, including a gas diffusion layer, a Ni foam layer and a catalyst layer. The Ni foam was subject to ultrasound treatment in 0.1 M HCl, H_2O and ethanol consecutively, and vacuum dried at 80 °C for 4 h. The catalyst layer was prepared by mixing the NCA_{LR}/Fe catalyst obtained above (or commercial Pt/C), acetylene black (as a conductive agent), and PTFE (as a binder) at the mass ratio of 6:1:3. The total thickness of the cathode was ca. 0.4 mm after compression with a manual tablet machine and vacuum dried at 80 °C for 4 h.

Results and discussion

The preparation of starch-derived, N-doped carbon aerogels embedded with single Fe atoms (NCA_{ST}/Fe) is schematically illustrated in Fig. 1a-1c, where three kinds of biomass starch hydrogels were prepared from edible lotus root, sweet potato and potato, and employed as 3D templates, with melamine as the N source (Fig. 1a and 1b). Experimentally, a starch

dispersion containing SiO_2 nanoparticles (15 nm), melamine, and Fe^{2+} were self-assembled into 3D hydrogels at 90 °C via noncovalent interactions (denoted as ST-Si/Me-Fe hydrogel, Fig. S1). The morphological information of the starch-derived hydrogels was investigated by SEM measurements. Pure lotus root hydrogel consists of interconnected micro-cavities of 20–50 μm in size, forming a honeycomb-like 3D framework (Fig. S2). After the incorporation of SiO_2 nanoparticles and melamine-Fe complex, the resulting hydrogel maintained the honeycomb-like 3D framework except for a rougher surface (Fig. 1d). The structure of the lotus root hydrogels (Fig. 1d inset) was then characterized by FTIR spectroscopic measurements. It can be seen that the amide II band (1546 cm^{-1}) became weakened with the addition of $FeCl_2$ into the hydrogels (e.g., LR-Si/Me vs LR-Si/Me-Fe, Fig. S3), suggesting complexation between the metal atoms and amides of melamine. Consistent results are obtained in UV-vis absorption measurements (Fig. S4). Such strong interactions between melamine and Fe^{2+} may play a significant role in the incorporation of the metal centers into the carbon matrix and inhibition of metal aggregation during pyrolysis.

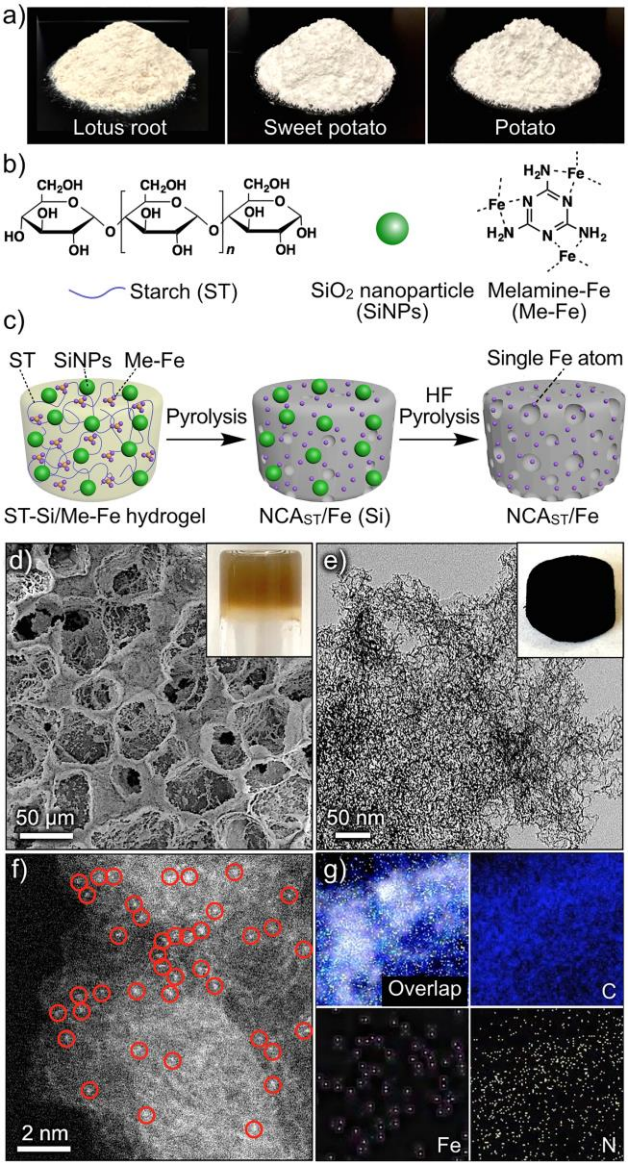

Fig. 1. (a) Digital photos of lotus root, sweet potato and potato starch. (b) Chemical structure of the starch (left), schematics for SiO_2 nanoparticles (middle) and chemical structure of the Me-Fe complex (right). (c) Schematic illustration for the synthesis of single Fe metal atoms dispersed in N-doped carbon aerogels (NCA_{ST}/Fe). (d) SEM image of the LR-Si/Me-Fe hydrogel; inset: digital photo of the LR-Si/Me-Fe hydrogel. (e) TEM image of NCA_{LR}/Fe; inset is the corresponding digital photo. (f) HAADF-STEM image of the NCA_{LR}/Fe aerogel. The red cycles indicate single Fe atoms. (g) Elemental maps of NCA_{LR}/Fe aerogel.

These ST-Si/Me-Fe hydrogels were then used as precursors to prepare NCA_{ST}/Fe (i.e., NCA_{LR}/Fe, NCA_{SP}/Fe, and NCA_{PT}/Fe). The fabrication procedure entails three major steps: (a) pyrolysis for creating microporous defects and heteroatom doping, (b) HF etching for removing SiO_2 nanoparticle templates and (c) second pyrolysis for improving conductivity (Fig. 1c and S1d). Taking NCA_{LR}/Fe (Fig. 1e inset) as the example, one can see that the sample exhibits a 3D hierarchical porous carbon structure, which is especially rich in pores of about 10 nm (Fig. 1e and S5).[42] In addition, in high angle annular dark field-scanning TEM (HAADF-STEM) studies, a large number of single metal atoms of about 2 Å in size within the porous carbon can be identified with the NCA_{ST}/Fe series (Fig. 1f and S6), in good agreement with results from bright-field STEM studies. The corresponding elemental mapping analysis shows that abundant N and Fe atoms were indeed successfully doped into the carbon skeletons without apparent agglomeration (Fig. 1g). Taken together, these results indicate successful preparation of Fe-N-C aerogel composites from biomass hydrogels with atomically dispersed Fe centers.

The elemental composition of the carbon aerogels were then examined by XPS, EDS and ICP-OES measurements. Take the lotus root-based aerogel as the example. Results from XPS and EDS measurements show that NCA_{LR}/Fe contains ca. 0.34 at.% of Fe and a relatively higher concentration of N (2.74 at.%) (Fig. S7 and S8, Table S1 and S2). From ICP-OES measurements, the Fe content in NCA_{LR}/Fe is ca. 1.3 wt.%, which is ca. 22 times higher than that of CA_{LR}/Fe (0.06 wt. %, Table S3). This indicates that melamine (and the resulting N dopants) plays a vital role in anchoring/stabilizing single Fe atoms within the carbon aerogels (and hence the generation of ORR active sites, *vide infra*).

Another key factor in the formation of single metal sites is the carbon micropores.[43] N_2 adsorption-desorption isotherm measurements were then performed to examine the porosity of these carbon aerogels. As listed in Table S4, whereas micropores account for only 19.8% of the total pore volume of the CA_{LR} sample, the NCA_{LR} sample exhibits a much larger percentage of micropore volume at 36.1%, and NCA_{LR}/Fe at 24.2 % (Fig. 2a and S9). This suggests that melamine can facilitate the generation of micropores during graphitization of starch chains at elevated temperatures. It is likely that the resulting microporous defects helped capture and stabilize the mobile single Fe atoms via physical and chemical interactions. This result can be conversely proved by the fact that merely 0.06 wt.% metal atoms were captured into the carbon matrix of CA_{LR}/Fe which was prepared without the melamine precursor. In addition, due to the plugging effects of the *in situ* formed

single metal sites, the Fe atoms mostly appear near the edges of the micropores (white areas in Fig. 1f and S6a), which can be readily accessible during catalytic reactions.[44, 45]

Notably, the NCA_{LR}/Fe aerogel consists of a 3D hierarchical, porous network (inset to Fig. 2a), with a high Brunauer-Emmett-Teller (BET) specific surface area of 699.8 m^2 g^{-1} that is anticipated to facilitate effective mass transfer during ORR.[46, 47] Raman spectroscopic measurements (Fig. S10) show that the ratio of the D and G band intensity (I_D/I_G) increases slightly from 0.97 for CA_{LR} to 1.19 for NCA_{LR}/Fe, indicative of a small increase of structural defects induced by single Fe atoms doped in the carbon matrix.[48] In fact, a pronounced 2D peak appears around 2672 cm^{-1} in the NCA_{LR}/Fe aerogel, but is absent in other samples without metal doping. This suggests that Fe doping is conducive to the generation of ultrathin graphite carbon, which is favorable to electron transfer.[49] From XPS measurements (Fig. S11), both Fe(II) and Fe(III) species can be identified in the NCA_{LR}/Fe sample, with two doublets at 710.8/722.8 eV and 713.6/725.2 eV, respectively; and in the corresponding scan of the N 1s electrons (Fig. 2b), the Fe–N peak can be deconvoluted at 399.2 eV, in addition to the graphitic, pyridinic, pyrrolic and oxidized N species that are also apparent in the Fe-free NCA_{LR}, indicating successful formation of FeN_x moieties in the NCA_{LR}/Fe aerogel.[50]

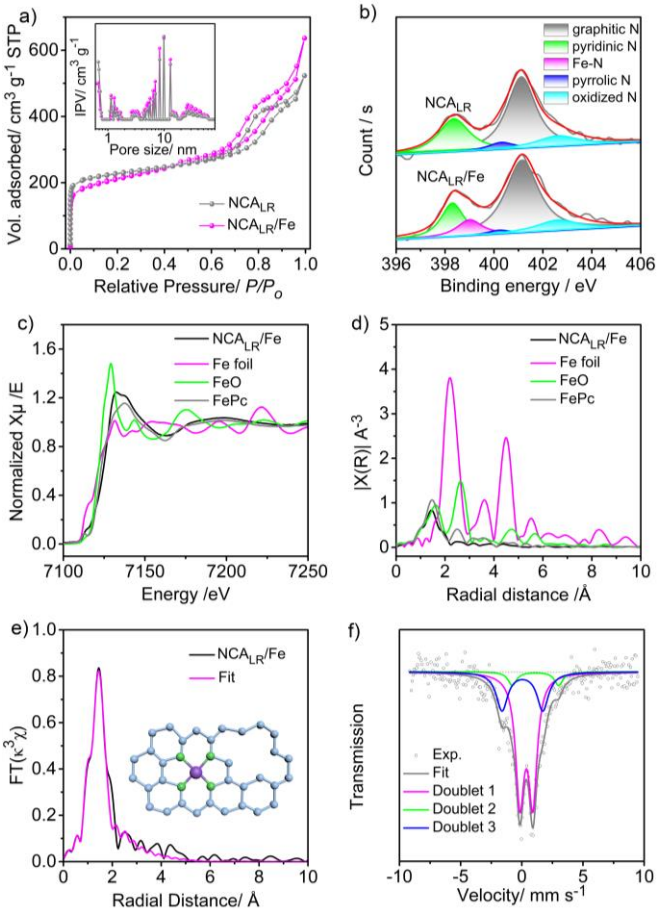

Fig. 2. (a) N_2 adsorption-desorption isotherm of NCA_{LR} and NCA_{LR}/Fe. Inset is the corresponding pore size distribution. (b) XPS spectra of the N 1s electrons in NCA_{LR} and NCA_{LR}/Fe. (c) K-edge XANES of NCA_{LR}/Fe and Fe foil. (d) K-edge EXAFS of NCA_{LR}/Fe and Fe foil. (e) Corresponding EXAFS spectrum and fitting curve for NCA_{LR}/Fe. Inset is a schematic of the FeN_4 structure within a defective carbon substrate. (f) ^{57}Fe Mössbauer spectrum and fittings of the NCA_{LR}/Fe aerogel.

XAS measurements were then carried out to investigate the atomic configuration of the FeN_x centers.[51] As shown in Fig. 2c, the Fe K-edge X-ray absorption near-edge structure (XANES) spectrum of the NCA_{LR}/Fe aerogel is significantly different from those of Fe foil and FeO, but very similar to that of FePc, consistent with the formation of FeN_x moieties in the sample.[52] The extended X-ray absorption fine structure (EXAFS) of the Fe foil shows a strong peak at 2.2 Å due to the Fe-Fe bond, which is absent in NCA_{LR}/Fe. In addition, the Fe–O bond (1.63 Å), which is apparent with FeO, is not observed with NCA_{LR}/Fe, either.[52, 53] These observations indicate that Fe was indeed atomically dispersed in the carbon matrix, with no aggregation, consistent with results from HAADF-STEM (Fig. 1 and S6) and XRD measurements (Fig. 2d and S12). In fact, the NCA_{LR}/Fe sample exhibits only a prominent peak at 1.45 Å, very consistent with the Fe–N bond as observed with FePc, implying a similar coordination structure of the metal centers between these two samples. In fact, the first shell of NCA_{LR}/Fe can be well-fitted with approximately four N atoms at a bond length of 1.97 Å, indicating the formation of monodisperse FeN_4 units in the carbon matrix (Fig. 2e and Table S5). This result was further confirmed by Mössbauer spectroscopy measurements. As shown in Fig. 2f, three doublets (D1, D2 and D3) can be seen and attributed to square planar Fe(II)N_4, with Fe(II) in low (65.83 %), medium (7.12 %) and high (27.06 %) spins, respectively, confirming the formation of stable FeN_4 active centers.[19] Taken together, results from these measurements indicate that the FeN_4 active sites are indeed formed and stabilized by microporous defects in the carbon aerogels.The electrocatalytic activities of the obtained aerogels were then examined by using RDE voltammetry in O_2-saturated 0.1 M KOH. As shown in Fig. 3a-c, NCA_{LR}/Fe, NCA_{SP}/Fe and NCA_{PT}/Fe all show similar, excellent catalytic activities towards ORR with onset potentials (E_{onset} = +1.05 V, +1.02 V and +1.05 V vs RHE, respectively) and half-wave potentials ($E_{1/2}$ = +0.88 V, +0.87 V and +0.88 V, respectively) that are all more positive than those of commercial 20 wt. % Pt/C (+0.99 V, 0.84 V). This is likely due to the formation of FeN_4 moieties in the biomass-derived, hierarchical porous carbon aerogels.[46, 47] (Given the similar ORR performance of these three catalysts, hereinafter we would use NCA_{LR}/Fe as the example to gain deeper insights into the catalytic performance of these biomass-derived aerogels.)

The ORR activity is markedly lower with carbon aerogel (CA_{LR}) that is free of N and Fe doping, which shows a markedly more negative E_{onset} of +0.83 V and $E_{½}$ of +0.70 V, indicating that porous carbon aerogel alone is inadequate to catalyze ORR (Fig. 3b). The performance was improved somewhat by the doping of N atoms into the porous carbon, as the NCA_{LR} aerogel shows a positive shift of $E_{½}$ by about 30 mV.[54-56] As for the CA_{LR}/Fe sample, it only shows negligible improvement of the ORR activity, likely due to the lack of microporous defects that limits the incorporation of individual Fe atoms into the carbon aerogels. By sharp contrast, the ORR performance was significantly enhanced when both Fe and N dopants were

incorporated into the carbon aerogel. For instance, the E_{onset} and $E_{½}$ of NCA_{LR}/Fe are both even more positive than those of Pt/C (Fig. 3c),[57] and among the best ORR catalysts based on transition metals-doped carbon reported in recent literature (Table S6).[52, 58] Such a remarkable catalytic activity of the NCA_{LR}/Fe sample highlights the important role of melamine-induced microporous defects in the stabilization of individual Fe atoms in the carbon matrix.

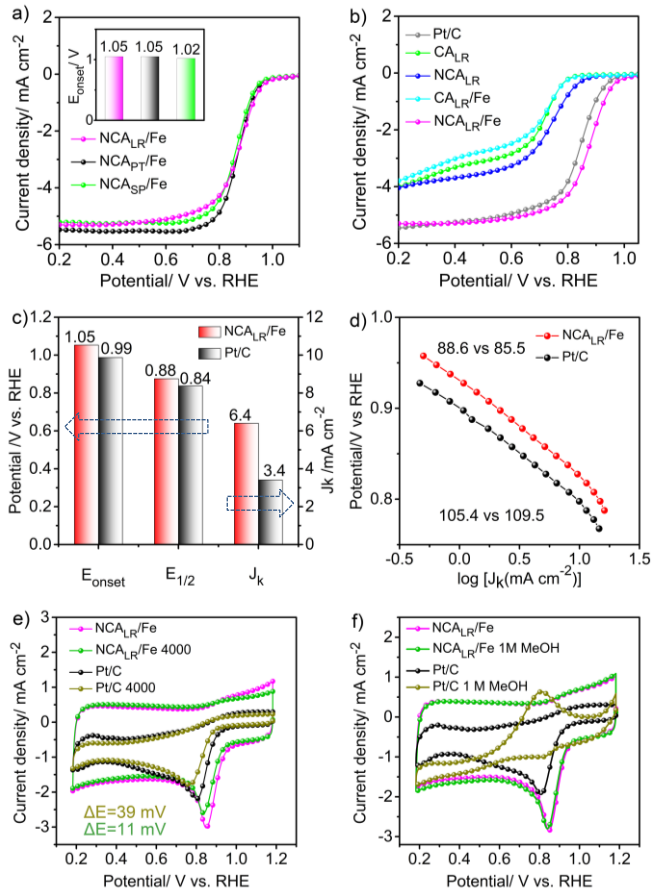

Fig. 3. (a) and (b) LSV curves of the various carbon aerogels as well as the Pt/C as ORR catalysts at 1600 rpm and 5 mV s^{-1}. (c) E_{onset}, $E_{1/2}$ and J_k (at +0.85 V) of the NCA_{LR}/Fe carbon aerogel catalyst and Pt/C. (d) Tafel plots of NCA_{LR}/Fe and Pt/C in O_2-saturated 0.1 M KOH. (e) Durability tests of NCA_{LR}/Fe and Pt/C; scan rate: 50 mV s^{-1}, medium: O_2-saturated 0.1 M KOH. (f) CV curves of the NCA_{LR}/Fe and commercial Pt/C as ORR catalysts in the presence or absence of 1 M MeOH.

From the corresponding Koutecky-Levich plots (Fig. S13), the average number of electron transfer (n) involved in ORR is estimated to be *ca*. 3.90 with NCA_{LR}/Fe, markedly higher than those of others in the series, suggesting a highly efficient $4e^-$ reaction pathway in oxygen reduction (Fig. S14 and Table S7). The corresponding kinetic current density (J_k) at +0.85 V is estimated to be 6.4 mA cm^{-2} of the NCA_{LR}/Fe sample, almost twice that of Pt/C (3.4 mA cm^{-2}, Fig. 3c). Fig. 3d shows the corresponding Tafel plots, where the NCA_{LR}/Fe aerogel can be seen to exhibit a Tafel slope of 88.6 mV dec^{-1}, very close to that of Pt/C (85.6 mV dec^{-1}), suggestive of a similar kinetic process between these two catalysts. It should be noted that the Tafel slopes for ORR are generally observed at 60 or 120 mV/dec. In the former the rate determining step is thought to be a pseudo two-electron reaction, whereas in the latter the first-electron reduction of oxygen.[59] This suggests that both reactions likely play a significant role in ORR catalyzed by the NCA_{LR}/Fe aerogel.[59]

To examine the durability of the NCA_{LR}/Fe catalyst, cyclic voltammetry measurements within the potential range of +0.1 V to +0.5 V was performed. As shown in Fig. 3e, the peak potential of oxygen reduction shifts negatively by only 11 mV after 4000 cycles with the NCA_{LR}/Fe sample, much smaller than that observed with Pt/C (39 mV) under the same conditions, indicative of much better durability of the former. In addition, the peak current at the NCA_{LR}/Fe catalyst remains virtually unchanged upon the addition of methanol (1.0 M) into the electrolyte, whereas significant methanol poisoning can be seen with Pt/C, confirming much enhanced tolerance of NCA_{LR}/Fe against methanol crossover (Fig. 3f). In addition, apparent activity is also observed with NCA_{LR}/Fe in acidic media (Fig. S15, S16 and Table S8).

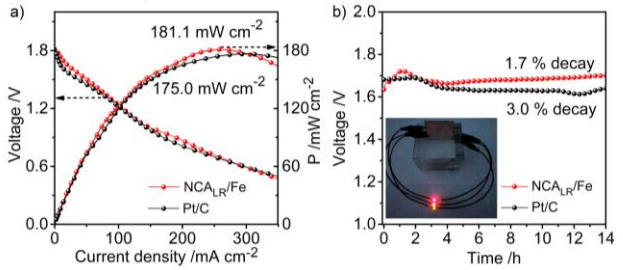

Fig. 4. (a) Polarization curves and power density plots of the NCA_{LR}/Fe and Pt/C catalysts. (b) Constant current discharge tests at the current density of 20 mA cm^{-2}; inset: Photo of parallel red, yellow and green LEDs (rated voltages of 1.8 V to 2.0 V) simultaneously powered by only one Al-air battery assembled by NCA_{LR}/Fe).

The practical application of the NCA_{LR}/Fe catalyst was then evaluated with a home-made Al-air battery using 6 M KOH as the electrolyte.[28, 60] Note that in 6 M KOH, NCA_{LR}/Fe still outperforms Pt/C towards ORR, with a reduction peak potential of +0.869 V that is about 30 mV more positive (Fig. S17). For the Al-air battery fabricated with a NCA_{LR}/Fe cathode, the open circuit voltage is estimated to be 1.81 V, and peak power density 181.1 mW cm^{-2}, which are 10 mV and 6 mW cm^{-2} higher than those of the battery with a Pt/C cathode (Fig. 4a and S18). Note that the performance of the NCA_{LR}/Fe Al-air battery also surpasses relevant results reported in recent literature (Table S9).

In fact, only one NCA_{LR}/Fe Al-air battery is needed to power up three red, yellow and green LEDs in parallel with rated voltages of 1.8 V to 2.0 V (inset to Fig. 4b), attesting its high open circuit voltage. In addition, after discharging at the constant current density of 20 mA cm^{-2} for 14 h, the NCA_{LR}/Fe battery exhibits only a 1.7 % voltage decay, in contrast to 3.0 % for the Pt/C battery (Fig. 4b). All these results reconfirm the remarkable activity and durability of the NCA_{LR}/Fe aerogel catalysts, highlighting their great potential application in metal-air batteries.

Conclusions

In this study, we developed a facile approach to the mass production of 3D porous carbon aerogels embedded with abundant single Fe atoms by tailoring biomass hydrogel precursors. Single Fe atoms were captured and stabilized within the porous carbon aerogels by *in situ* formed microporous defects, leading to the formation of highly active FeN_4 catalytic sites, as manifested in BET, XPS, XAS and Mössbauer spectroscopic measurements. Electrochemical tests showed a superior catalytic performance of the aerogel catalysts, as compared to commercial Pt/C, within the context of onset potential, half-wave potential, methanol tolerance, and durability. The practical application of the aerogel catalysts was further demonstrated as the cathode catalysts for Al-air battery, which exhibited a higher open circuit voltage, power density and more stable discharge voltage than that that with a Pt/C cathode. Results from the present study may pave a new pathway for the rational design and engineering of low-cost, high-performance electrocatalysts based on abundant biomass.

Conflicts of interest

There are no conflicts to declare.

Acknowledgements

This work was supported by the National Natural Science Foundation of China (21773311, 21473257); Hunan Provincial Science and Technology Plan Project of China (2016TP1007); Special Program for Applied Research on Super Computation of the NSFC-Guangdong Joint Fund (the second phase). S. W. C. thanks the National Science Foundation for partial support of the work (CHE-1710408 and CHE-1900235). T. H. thanks a research fellowship from the China Scholarship Council.

References

1. X. Cao, C. Tan, M. Sindoro and H. Zhang, *Chem. Soc. Rev.*, 2017, **46**, 2660-2677.
2. P. Li and H. C. Zeng, *Adv. Funct. Mater.*, 2017, **27**, 1606325.
3. C. Tang and Q. Zhang, *Adv. Mater.*, 2017, **29**, 1604103.
4. L. Wang, Y. Wang, M. Wu, Z. Wei, C. Cui, M. Mao, J. Zhang, X. Han, Q. Liu and J. Ma, *Small*, 2018, **14**, 1800737.
5. N. Xu, Y. Zhang, T. Zhang, Y. Liu and J. Qiao, *Nano Energy*, 2019, **57**, 176-185.
6. C. Hu, Y. Xiao, Y. Zou and L. Dai, *Electrochem. Energy Rev.*, 2018, **1**, 84-112.
7. X. Huang, Z. Zhao, L. Cao, Y. Chen, E. Zhu, Z. Lin, M. Li, A. Yan, A. Zettl, Y. M. Wang, X. Duan, T. Mueller and Y. Huang, *Science*, 2015, **348**, 1230-1234.
8. Z. Wang, H. Jin, T. Meng, K. Liao, W. Meng, J. Yang, D. He, Y. Xiong and S. Mu, *Adv. Funct. Mater.*, 2018, **28**, 1802596.
9. D. Liu, B. Wang, H. Li, S. Huang, M. Liu, J. Wang, Q. Wang, J. Zhang and Y. Zhao, *Nano Energy*, 2019, **58**, 277-283.
10. G. Wu, K. L. More, C. M. Johnston and P. Zelenay, *Science*, 2011, **332**, 443-447.
11. M. Wu, Y. Wang, Z. Wei, L. Wang, M. Zhuo, J. Zhang, X. Han and J. Ma, *J. Mater. Chem. A*, 2018, **6**, 10918-10925.
12. Y. He, Q. Tan, L. Lu, J. Sokolowski and G. Wu, *Electrochem. Energy Rev.*, 2019, **2**, 231-251.
13. L. Yang, J. Yu, Z. Wei, G. Li, L. Cao, W. Zhou and S. Chen, *Nano Energy*, 2017, **41**, 772-779.
14. G. Wu, W. Chen, X. Zheng, D. He, Y. Luo, X. Wang, J. Yang, Y. Wu, W. Yan, Z. Zhuang, X. Hong and Y. Li, *Nano Energy*, 2017, **38**, 167-174.
15. W. Chen and S. Chen, *Angew. Chem. Int. Ed.*, 2009, **48**, 4386-4389.
16. Y. Fan, S. Ida, A. Staykov, T. Akbay, H. Hagiwara, J. Matsuda, K. Kaneko and T. Ishihara, *Small*, 2017, **13**, 1700099.
17. X. X. Wang, D. A. Cullen, Y.-T. Pan, S. Hwang, M. Wang, Z. Feng, J. Wang, M. H. Engelhard, H. Zhang, Y. He, Y. Shao, D. Su, K. L. More, J. S. Spendelow and G. Wu, *Adv. Mater.*, 2018, **30**, 1706758.
18. Q. Jia, S. Ghoshal, J. Li, W. Liang, G. Meng, H. Che, S. Zhang, Z. Ma and S. Mukerjee, *J. Am. Chem. Soc.*, 2017, **139**, 7893-7903.
19. J. Wang, Z. Huang, W. Liu, C. Chang, H. Tang, Z. Li, W. Chen, C. Jia, T. Yao, S. Wei, Y. Wu and Y. Li, *J. Am. Chem. Soc.* , 2017, **139**, 17281-17284.
20. Y. Qiao, P. Yuan, Y. Hu, J. Zhang, S. Mu, J. Zhou, H. Li, H. Xia, J. He and Q. Xu, *Adv. Mater.*, 2018, **30**, 1804504.
21. Y. Sun, X. Zhang, M. Luo, X. Chen, L. Wang, Y. Li, M. Li, Y. Qin, C. Li, N. Xu, G. Lu, P. Gao and S. Guo, *Adv. Mater.*, 2018, **30**, 1802136.
22. I. Ahmad, F. Li, C. Kim, J.-M. Seo, G. Kim, J. Mahmood, H. Y. Jeong and J.-B. Baek, *Nano Energy*, 2019, **56**, 581-587.
23. W. Zhao, K. Huang, Q. Zhang, H. Wu, L. Gu, K. Yao, Y. Shen and Y. Shao, *Nano Energy*, 2019, **58**, 69-77.
24. J. Jones, H. Xiong, A. T. DeLaRiva, E. J. Peterson, H. Pham, S. R. Challa, G. Qi, S. Oh, M. H. Wiebenga, X. I. Pereira Hernández, Y. Wang and A. K. Datye, *Science*, 2016, **353**, 150-154.
25. P. Szuromi, *Science*, 2016, **353**, 133-133.
26. Y. Peng, B. Lu and S. Chen, *Adv. Mater.*, 2018, **30**, 1801995.
27. J. Han, X. Meng, L. Lu, J. Bian, Z. Li and C. Sun, *Adv. Funct. Mater.*, 2019, **29**, 1808872.
28. S. Li, C. Cheng, X. Zhao, J. Schmidt and A. Thomas, *Angew. Chem.*, 2018, **130**, 1874-1880.
29. Z. Zhang, X. Gao, M. Dou, J. Ji and F. Wang, *Small*, 2017, **13**, 1604290.
30. J. Ma, X. Wang, T. He, M. Tan, J. Zheng, H. Wu, M. Yuan, R. Shen, Y. Zhang and J. Xiang, *Dalton Trans.*, 2017, **46**, 6163-6167.
31. Y. Zheng, Y. Jiao, Y. Zhu, Q. Cai, A. Vasileff, L. H. Li, Y. Han, Y. Chen and S.-Z. Qiao, *J. Am. Chem. Soc.* , 2017, **139**, 3336-3339.
32. J. Wei, Y. Hu, Y. Liang, B. Kong, Z. Zheng, J. Zhang, S. P. Jiang, Y. Zhao and H. Wang, *J. Mater. Chem. A*, 2017, **5**, 10182-10189.
33. C. L. Zhang, B. R. Lu, F. H. Cao, Z. Y. Wu, W. Zhang, H. P. Cong and S. H. Yu, *Nano Energy*, 2019, **55**, 226-233.
34. H. Cong, J. Chen and S. Yu, *Chem. Soc. Rev.*, 2014, **43**, 7295-7325.
35. Z. Wu, S. Yang, Y. Sun, K. Parvez, X. Feng and K. Müllen, *J. Am. Chem. Soc.*, 2012, **134**, 9082-9085.
36. C. Ziegler, A. Wolf, W. Liu, A.-K. Herrmann, N. Gaponik and A. Eychmüller, *Angew. Chem. Int. Ed.*, 2017, **56**, 13200-13221.
37. B. Cai, R. Hübner, K. Sasaki, Y. Zhang, D. Su, C. Ziegler, M. B. Vukmirovic, B. Rellinghaus, R. R. Adzic and A. Eychmüller, *Angew. Chem. Int. Ed.*, 2018, **57**, 2963-2966.
38. L. Zhang, T. Liu, N. Chen, Y. Jia, R. Cai, W. Theis, X. Yang, Y. Xia, D. Yang and X. Yao, *J. Mater. Chem. A*, 2018, **6**, 18417-18425.
39. L. E. Buerkle and S. J. Rowan, *Chem. Soc. Rev.*, 2012, **41**, 6089-6102.
40. N. M. Sangeetha and U. Maitra, *Chem. Soc. Rev.*, 2005, **34**, 821-836.

41. K. Parvez, S. Yang, Y. Hernandez, A. Winter, A. Turchanin, X. Feng and K. Müllen, *ACS Nano*, 2012, **6**, 9541-9550.
42. D. Yan, Y. Li, J. Huo, R. Chen, L. Dai and S. Wang, *Adv. Mater.*, 2017, **29**, 1606459.
43. Y. Zhao, X. Li, X. Jia and S. Gao, *Nano Energy*, 2019, **58**, 384-391.
44. J. Pandey, B. Hua, W. Ng, Y. Yang, K. van der Veen, J. Chen, N. J. Geels, J.-L. Luo, G. Rothenberg and N. Yan, *Green Chem.*, 2017, **19**, 2793-2797.
45. X. Fu, N. Li, B. Ren, G. Jiang, Y. Liu, F. M. Hassan, D. Su, J. Zhu, L. Yang, Z. Bai, Z. P. Cano, A. Yu and Z. Chen, *Adv. Energy Mater.*, 2018, **9**, 1803737.
46. L. Shao, S. Wang, M. Liu, J. Huang and Y. Liu, *Chem. Eng. J.*, 2018, **339**, 509-518.
47. L. Shao, Y. Li, J. Huang and Y. Liu, *Ind. Eng. Chem. Res.*, 2018, **57**, 2856-2865.
48. T. He, H. Xue, X. Wang, S. He, Y. Lei, Y. Zhang, R. Shen, Y. Zhang and J. Xiang, *Nanoscale*, 2017, **9**, 8341-8348.
49. Z. Sun, Z. Yan, J. Yao, E. Beitler, Y. Zhu and J. M. Tour, *Nature*, 2010, **468**, 549.
50. B. Z. Lu, T. J. Smart, D. D. Qin, J. E. Lu, N. Wang, L. M. Chen, Y. Peng, Y. Ping and S. W. Chen, *Chem. Mater.*, 2017, **29**, 5617-5628.
51. J. Liu, M. Jiao, L. Lu, H. M. Barkholtz, Y. Li, Y. Wang, L. Jiang, Z. Wu, D.-j. Liu, L. Zhuang, C. Ma, J. Zeng, B. Zhang, D. Su, P. Song, W. Xing, W. Xu, Y. Wang, Z. Jiang and G. Sun, *Nat. Commun.*, 2017, **8**, 15938.
52. Y. Chen, S. Ji, Y. Wang, J. Dong, W. Chen, Z. Li, R. Shen, L. Zheng, Z. Zhuang, D. Wang and Y. Li, *Angew. Chem. Int. Ed.*, 2017, **56**, 6937-6941.
53. H. H. Zhang, Sooyeon Wang, Maoyu , Z. S. K. Feng, L. Q. Luo, Zhi Xie, Xiaohong and C. S. Wang, Dong Shao, Yuyan and Wu, Gang *J. Am. Chem. Soc.*, 2017, **139**, 14143-14149.
54. J. Shi, M. Fan, J. Qiao and Y. Liu, *Chem. Lett.*, 2014, **43**, 1484-1486.
55. Q. Tang, L. Wang, M. Wu, N. Xu, L. Jiang and J. Qiao, *J. Power Sources*, 2017, **365**, 348-353.
56. M. Wu, J. Qiao, K. Li, X. Zhou, Y. Liu and J. Zhang, *Green Chem.*, 2016, **18**, 2699-2709.
57. W. Xia, A. Mahmood, Z. Liang, R. Zou and S. Guo, *Angew. Chem. Int. Ed.* , 2016, **55**, 2650-2676.
58. P. Yin, T. Yao, Y. Wu, L. Zheng, Y. Lin, W. Liu, H. Ju, J. Zhu, X. Hong, Z. Deng, G. Zhou, S. Wei and Y. Li, *Angew. Chem. Int. Ed.* , 2016, **55**, 10800-10805.
59. G. He, Y. Song, K. Liu, A. Walter, S. Chen and S. Chen, *ACS Catal.*, 2013, **3**, 831-838.
60. J. Li, Z. Zhou, K. Liu, F. Li, Z. Peng, Y. Tang and H. Wang, *J. Power Sources*, 2017, **343**, 30-38.

TOC

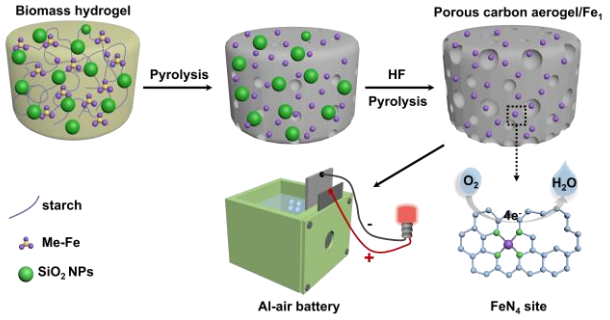

Biomass-derived carbon aerogel with hierarchical porosity and FeN_4 single atom sites outperforms platinum towards oxygen reduction reaction in alkaline media and can be used as the cathode catalyst for aluminium-air battery.